

Multi-phase environment of compact galactic nuclei: the role of the Nuclear Star Cluster

A. Różańska,¹ D. Kunneriath,^{2,3} B. Czerny,^{4,1} T. P. Adhikari,¹ and V. Karas³

¹*Nicolaus Copernicus Astronomical Center, Polish Academy of Sciences, Bartycka 18, 00-716 Warsaw, Poland*

²*National Radio Astronomy Observatory, 520 Edgemont Road, Charlottesville 22903, VA, USA*

³*Astronomical Institute, Academy of Sciences, Boční II 1401, CZ-141 00 Prague, Czech Republic*

⁴*Center for Theoretical Physics, Polish Academy of Sciences, Al. Lotnikow 32/46, 02-668 Warsaw, Poland*

Accepted for publication in MNRAS

ABSTRACT

We study the conditions for the onset of Thermal Instability in the innermost regions of compact galactic nuclei, where the properties of the interstellar environment are governed by the interplay of quasi-spherical accretion onto a supermassive black hole (SMBH) and the heating/cooling processes of gas in a dense nuclear star cluster. Stellar winds are the source of material for radiatively inefficient (quasi-spherical, non-magnetised) inflow/outflow onto the central SMBH, where a stagnation point develops within the Bondi type accretion. We study the local thermal equilibrium to determine the parameter space which allows cold and hot phases in mutual contact to co-exist. We include the effects of mechanical heating by stellar winds and radiative cooling/heating by the ambient field of the dense star cluster. We consider two examples: the Nuclear Star Cluster (NSC) in the Milky Way central region (including the gaseous Mini-spiral of Sgr A*), and the Ultra-Compact Dwarf galaxy M60-UCD1. We find that the two systems behave in different ways because they are placed in different areas of parameter space in the instability diagram: gas temperature vs. dynamical ionization parameter. In the case of Sgr A*, stellar heating prevents the spontaneous formation of cold clouds. The plasma from stellar winds joins the hot X-ray emitting phase and forms an outflow. In M60-UCD1 our model predicts spontaneous formation of cold clouds in the inner part of the galaxy. These cold clouds may survive since the cooling timescale is shorter than the inflow/outflow timescale.

Key words: galaxies: active – galaxies: individual: M60-UCD1 – Galaxy: nucleus – instabilities

1 INTRODUCTION

The composition and state of interstellar gas and dust in galaxies vary across different morphological types and evolutionary stages (Binney & Merrifield 1998; Swamy 2005). New stars form if the building material is available but the process of star-formation can be quenched by shock-heating and lack of supplies as galaxies evolve in the course of cosmological history (Kennicutt 1998; Tacchella et al. 2015). The environmental aspects are particularly complex in the central regions of galaxies, where strong tidal fields as well as effects of intense irradiation arise in the sphere of influence of the supermassive black hole (SMBH). The latter usually resides within a dense Nuclear Star Cluster (NSC) that may or may not be permeated by the dusty gaseous environment, depending on the specific conditions of a given source (Cole & Debattista 2016).

Our Milky Way’s centre is a prominent example of a NSC that hosts both a SMBH and a large amount of material forming new stars even in its recent past (Eckart et al. 2005; Genzel et al. 2010). The physics of NSCs in galaxies, namely, their origin, history and the composition of their interstellar environment has a close re-

semblance on smaller scales to the properties of globular clusters (de Grijs & Lépine 2010). Unlike nuclei of galaxies, typical globular clusters lack SMBHs in their cores; also, they are generally unable to retain any significant amount of gas and dust (Frank & Gisler 1976; Moore & Bildsten 2011). However, the category of Ultra-Compact Dwarf galaxies (Mieske et al. 2013; Mieske 2014) appears to be a suitable type of object that can help us to explore the physics and evolution of NSCs with a central SMBH, and to compare them with the properties of the NSC in our Galaxy.

The mechanism of cooling and heating of the interstellar medium (ISM) has been the object of detailed studies for some time (Dyson & Williams 1980; Kennicutt et al. 1998). The microscopic processes that govern the gas dynamics are well understood, but nevertheless we still lack a detailed understanding of the chemical composition of the dusty plasma and of the energy input from stars. Such processes in galactic cores are complicated further by the unusually high density of the NSC (Genzel et al. 2010; Schödel et al. 2014; Fritz et al. 2016), the effect of accretion onto SMBH and possible feedback in the form of a jet (Mościbrodzka & Proga 2013;

Yuan & Narayan 2014), vigorous starburst activities, as well as the role of interactions and mergers (Kennicutt & Evans 2012). In this paper, we consider length-scales deep inside the NSC, where radiation and outflows from stars as well as energetic emission from the accretion flow, govern the physical properties of the system (Dopita & Sutherland 2003).

The complexity of the gas dynamics in such a situation was described by Silich et al. (2008) in their spherically symmetric picture. Very close to the center the material flows in, and accretes onto the supermassive black hole. Far out the material has enough energy to escape in a transonic outflow, leading to a continuous loss of gas. If the radiative cooling is inefficient, the inflow/outflow regions are separated by a stagnation radius. The relevant solutions have been found by Quataert (2004). However, if plasma cooling is efficient, instead of a simple stagnation radius a whole region forms with no stationary solution (Silich et al. 2008). A multi-phase medium develops where cold (relatively dense) clouds can coexist together with the hot, diluted gas (Róžańska et al. 2014). Pressure is the same in both phases. Therefore, density and temperature can span a broad range of values. The fate of the cold phase is determined by the characteristic length (Field 1965; Defouw 1970; Begelman & McKee 1990),

$$\lambda_F = \left(\frac{\kappa T}{\Lambda n^2} \right)^{1/2}, \quad (1)$$

where κ is the thermal conductivity of the medium, T – temperature, n – density number, and Λ is the total cooling rate (Draine & Giuliani 1984). Clouds of size less than λ_F tend to evaporate (heat conduction dominates), whereas larger clouds can be stabilized by radiative losses in the hot ambient medium (external heating vs. radiative cooling define the equilibrium of large clouds). Additional processes, such as turbulence and magnetic fields can further modify the basic scenario (small-scale magnetic fields induce anisotropy by inhibiting heat transport across the tangled field lines), but for the purpose of this paper we do not take them into account. Here we consider a local development of Thermal Instability (TI), although larger-scale global instabilities may also be important for the evolution of the system as a whole (Ciotti & Ostriker 2001).

We study the above-mentioned type of TI, paying attention to the description of the heating/cooling processes of matter with the use of the photoionization code CLOUDY (Ferland 1996; Ferland et al. 2013). A simple parametrization of the gas cooling rate from Plewa (1995) was employed by Silich et al. (2008), while we add a more detailed description of the system. In particular, we include the spectral shape of the incident radiation from NSC. Here, we consider two special cases. The first example concerns the dense NSC near the Galactic Center (GC) SMBH. In addition to our previous work (Czerny et al. 2013a,b; Róžańska et al. 2014) where we have taken into account the role of radiation heating by accretion flow, now we also include the role of energy input by radiation and wind outflows generated by hot stars. The second example falls within the category of Ultra-Compact Galaxies (UCDs) as an extreme case of NSCs where the outer part of the galaxy is missing, possibly due to interaction. In particular, the proto-typical M60-UCD1 (Mieske et al. 2013; Mieske 2014) serves as an exploratory case.

For their extreme properties – compact dimensions and enhanced mass-to-light ratio – UCDs fit somewhere in between the NSC of the Galactic centre on one side and globular clusters on the other. With respect to conditions for the TI, we expect different results for UCDs than for the GC of the Milky Way because

of their old stellar populations. By examining a sample of UCDs in the Virgo Cluster, Zhang et al. (2015a) concluded that these are a qualitatively different type of object from luminous (otherwise “normal”) globular clusters. Seth et al. (2014) has shown that the dynamical mass of M60-UCD1’s black hole reaches $2.1 \times 10^7 M_\odot$ while its nuclear star-cluster half-light radius is only ~ 24 pc. We illustrate the main differences of the plasma distribution in these type of objects from the case of our GC.

The structure of this paper is as follows. In Sec. 2 we introduce the basic equations and present the full set-up of our model. All results are shown in Sec. 3, where we discuss two examples: Sgr A* in the centre of the Milky Way, and UCD1 associated with M60 galaxy. Various aspects of the TI mechanism and potential ways to generalize our scenario are discussed in Sec. 4. Finally, Sec. 5 contains the main conclusions.

2 SET-UP OF THE MODEL

2.1 Conditions for Thermal Instability near SMBH

Multi-phase ISM can form spontaneously by the irradiation-induced effects of TI. The radiation field may originate from NSC stars or from the central accreting SMBH. Only a certain range of parameters allows TI to operate (e.g., Cox 2005, and further references therein). The essential parameters of our system are the distance from the centre, the accretion rate onto the black hole, the corresponding radiative efficiency of accretion, and the energy input and spectral distribution of stars in the NSC (Field 1965; Krolik et al. 1981; Róžańska & Czerny 1996). These complexities can be understood qualitatively: a clump of gas cools on a time-scale t_{cooling} , the exact value of which depends on the interplay of cooling mechanisms and their corresponding physical parameters such as: temperature, density, chemical abundances, and the dust content in ISM. Within the NSC, contact between the two phases (cold clumps embedded within a hot surrounding gas) is additionally affected by the continuous injection of fresh material in the form of stellar winds. This phenomenon of mass and energy input can lead to a stationary inflow/outflow solution, or a non-stationary process with a possibility of mass accumulation (Quataert 2004; Silich et al. 2004, 2008).

We simplify the description of the dynamics and analyze just the direction of the thermal evolution of the gas. Finally, we distinguish between two cases: the state of stable plasma in thermal equilibrium versus the cooling timescales relevant for plasma far from thermal equilibrium. The plasma cools via free-free emission, and by atomic bound-free processes and bound-bound transitions between different states. All these radiative cooling processes are included in the radiation transfer code CLOUDY.

2.2 Thermal equilibrium and the evolution timescale

Depending on the profile of the spectral energy distribution (SED), the incident radiation field can both cool and heat the plasma. The net effect is determined by plasma density as well as the spectral shape of the incident radiation. Thus, the presence of the radiation field contributes both to the cooling and heating rates, i.e., \mathcal{L} and \mathcal{H} , respectively in $\text{erg s}^{-1} \text{cm}^{-3}$. The difference between these two parameters describes the rate of exchange of total energy per unit volume by different cooling and heating processes.

We include the stellar emission from the NSC by modeling its

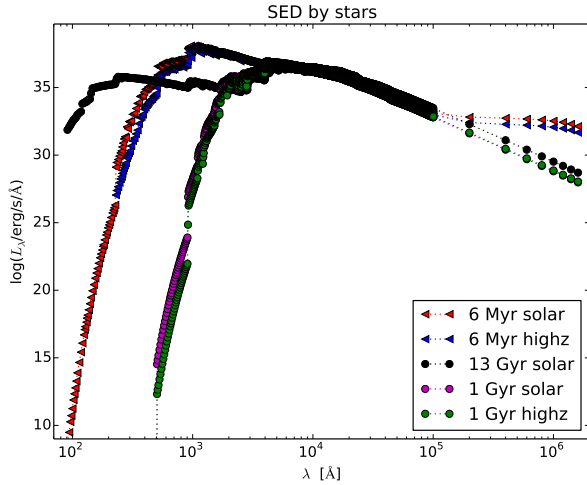


Figure 1. The broad band continua of the NSC stellar-energy distributions used in our computations. Red triangles represent the SED from the 6 Myr stellar population embedded within the NSC around Sgr A*, while black dots represent the SED for the 13 Gyr stellar population of M60-UCD1. This radiation component contributes to the cooling rate of the ISM compared to the mechanical heating by winds from the hot stars and by radiation originating from the central source of the SMBH accretion. In addition, the SED from a possible older, 1 Gyr, stellar population is presented by magenta dots, but the total luminosity of this cluster is two orders of magnitude lower and has no effect on TI of Sgr A*. For 6 Myr and 1 Gyr cases, solar versus increased metallicity are compared. An increase in metallicity of up to $z=0.04$ does not change the shape of the continuum significantly.

spectral shape appropriate for a given age. We also include the radiation produced by the accretion flow onto the central black hole, which is highly concentrated towards small radii. Nevertheless, our model is still an idealized scenario.

Similar processes of mass accumulation and generation of outflows with effects of stellar feedback have been explored on larger scales, typically from length-scales of several tens to several $\times 10^2$ pc (Schartmann et al. 2009), but in this paper we are interested only in the innermost regions of the NSC (typically a fraction of a parsec). For a given source our approach allows us to adjust the mechanical heating rate \mathcal{H} according to observational estimates.

We find the thermal equilibrium solution from the balance between all cooling and heating terms,

$$\dot{Q} = \mathcal{L} - \mathcal{H} = 0. \quad (2)$$

In a stationary system, the medium is thermally stable if the following condition for entropy perturbation ∂s is fulfilled (Dopita & Sutherland 2003, chapt. 7):

$$\frac{\partial(\dot{Q}/T)}{\partial s} > 0, \quad (3)$$

where \dot{Q} combines the heating and cooling mechanisms operating in the given system. For isobaric perturbations, Eq. (3) reduces to

$$\left. \frac{\partial \dot{Q}}{\partial T} \right|_P > 0, \quad (4)$$

which is equivalent to the original Field (1965) criterion, assuming the perfect gas equation of state.

To solve for the stability of the solution to Eq. (2), we employ CLOUDY 13.02 (Ferland et al. 2013), where the mechanical

volume heating is included through the appropriate option *Hextra* (see Hazy1 and Hazy2 documentation files), which reflects all possible heating of gas due to stellar winds of stars located within the region of consideration¹. This solution provides us with the local equilibrium temperature of the medium as a function of assumed ISM hydrogen density at a given location. The stability can be conveniently estimated from the diagram of stability curve. Note that in the definition of the ionization parameter Ξ (Tarter et al. 1969), we need to also include the luminosity of the stellar radiation field, which accounts for the gas ionization state:

$$\Xi = \frac{L_{\bullet} + L_{\text{stars}}}{4\pi c P_{\text{gas}} R^2}, \quad (5)$$

where L_{\bullet} is the accretion luminosity on to SMBH, L_{stars} is the stellar luminosity, P_{gas} is the local gas pressure, and R is the distance from the center. The curve Ξ vs. T indicates the thermal stability: in this relation, the branch with the positive slope is radiatively stable while the branch with the negative slope is unstable.

The cooling timescale to reach equilibrium (or time for a significant departure from it) is estimated as

$$t_{\text{cooling}} = \frac{E}{\mathcal{L}}. \quad (6)$$

In fact, this expression underestimates the actual timescales when the system is very close to thermal equilibrium, i.e. when $\mathcal{H} \approx \mathcal{L}$. Nonetheless, for a broad range of parameters, the cooling timescale is a reliable estimate of the rate at which TI develops in the system.

2.3 Non-equilibrium solutions

In general, the entropy s of matter evolves according to the equation

$$\frac{ds}{dt} = \frac{\mathcal{L} - \mathcal{H}}{nT} \propto \frac{1}{t_{\text{cooling}}}. \quad (7)$$

The corresponding timescale for cooling, t_{cooling} , now depends on the difference between the cooling and heating rates, $\mathcal{L} - \mathcal{H}$, and has to be calculated for initial conditions of the plasma far from thermal equilibrium. To streamline the analysis, the cooling timescale is frequently expressed as a function of temperature only.

For very short cooling times the initial perturbations condense rapidly into cold clumps, which then gradually fall down toward the centre in the gravitational field of the SMBH. In the opposite direction, bubbles of gas rise outwards in the hot phase. This is the same mechanism as the one operating in the context of intergalactic gas in galaxy clusters (McCourt et al. 2012). If the timescale to establish equilibrium greatly exceeds the dynamical timescale of accretion and/or outflow, named the crossing timescale t_{cross} , the supplied material cannot reach equilibrium temperature.

3 RESULTS

3.1 Case of Sgr A*

We assess the possibility of the existence of a multi-phase equilibrium taking into account three effects: (i) radiative heating by the accreting central black hole, as in Róžańska et al. (2014); (ii) additional radiative heating by stars; (iii) and mechanical heating by stellar winds.

Since Sgr A* was likely in much higher luminosity states in

¹ <http://www.nublado.org/>

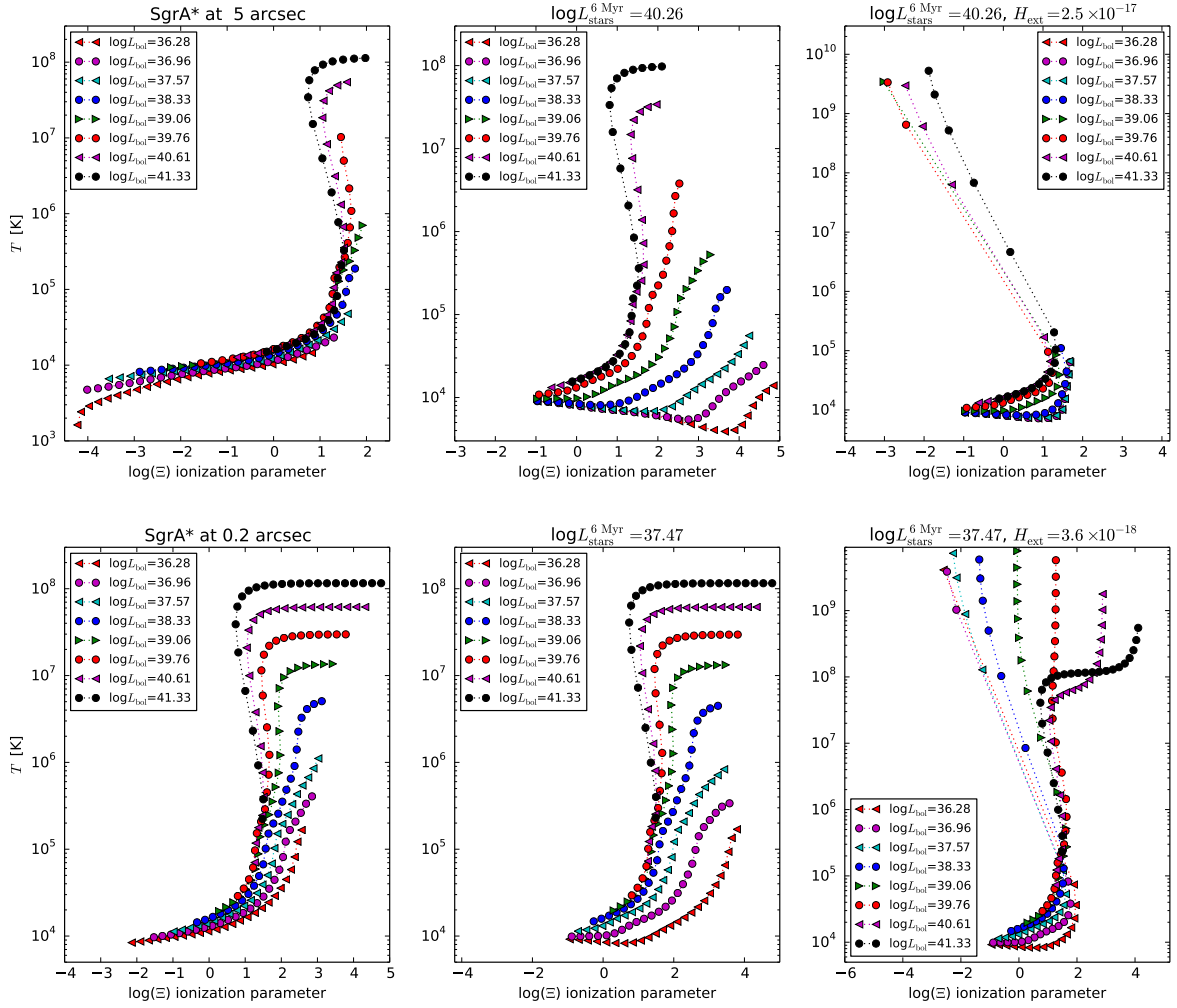


Figure 2. Solutions for S-curve of TI in the plane of temperature vs. ionization parameter, as defined in Eq. 5, for different luminosity states of the radiation: from the central source only (left panels), together with heating by stellar radiation (middle panels), and together with mechanical heating by winds (right panels). Values of central source luminosity are marked within the panels. We present results for the gas located at 5 arcsec from Sgr A* (upper row of panels) and at 0.2 arcsec (bottom row of panels). The luminosity and volume mechanical heating are $\log(L_{\text{stars}}/\text{erg s}^{-1}) = 40.03$ and $H_{\text{ext}} = 2.5 \times 10^{-17} \text{ erg s}^{-1} \text{ cm}^{-3}$, respectively, at 5 arcsec and $\log(L_{\text{stars}}/\text{erg s}^{-1}) = 37.47$ and $H_{\text{ext}} = 3.6 \times 10^{-18} \text{ erg s}^{-1} \text{ cm}^{-3}$, respectively, at 0.2 arcsec from Sgr A*.

the past several hundred years (see [Ponti et al. 2010](#), and references therein), we consider eight possible bolometric luminosities (always listed in the plots) of the central source, from the lowest one in quiescence: $\log(L_{\text{bol}}) = 36.28$, to the highest in the active phase: $\log(L_{\text{bol}}) = 41.33$ ([Zhang et al. 2015b](#); [Czerny et al. 2013b](#)). The spectral shape of the incident central emission depends on the bolometric luminosity. The final shape of the spectrum is computed from the theoretical model of radiatively inefficient Bondi accretion flow for eight values of the accretion rate. Spectra used for our photoionization calculations are the same as presented in Fig. 5 of [Mościbrodzka et al. \(2012\)](#).

We describe the stellar light using the spectral template for stars from STARBURST99 ([Leitherer et al. 1999](#); [Lu et al. 2013](#), see Fig. 1). As our basic model, we consider a young stellar population of 6 Myr stars with solar metallicity. We also checked the effect of higher metallicity stars and of the presence of an additional older stellar population of 1 Gyr stars. The normalization is set by the assumption that the total mass of the young NSC is $\sim 3.7 \times 10^4 M_{\odot}$

within 0.5 pc ([Lu et al. 2013](#)), whereas the total mass of old NSC is $\sim 8.0 \times 10^6 M_{\odot}$ within 2.5 pc ([Chatzopoulos et al. 2015](#)). The canonical spectral shape of stellar radiation used as an input to our CLOUDY simulations of the gas conditions around Sgr A* is presented in Fig. 1 by red triangles.

CLOUDY code always takes the illuminated source as a point source but the star cluster is an extended source, and the fraction of the ionization parameter, which is computed from the luminosity of stars, is constant over the whole NSC volume. Therefore, to ensure that the CLOUDY takes the same ionization parameter for all radii we within the nuclear cluster (which is physically consistent), we have to renormalise stellar luminosity depending on the distance, which is also an input parameter for CLOUDY simulations. In practice, we take the following steps: i) compute the SED for a given population and total mass of the NSC (given above) using Starburst99, ii) integrate this SED to obtain the total luminosity from all stars - L_{stars} , iii) assume that everywhere within the NSC gas "sees" the same amount of radiation, so the ionization

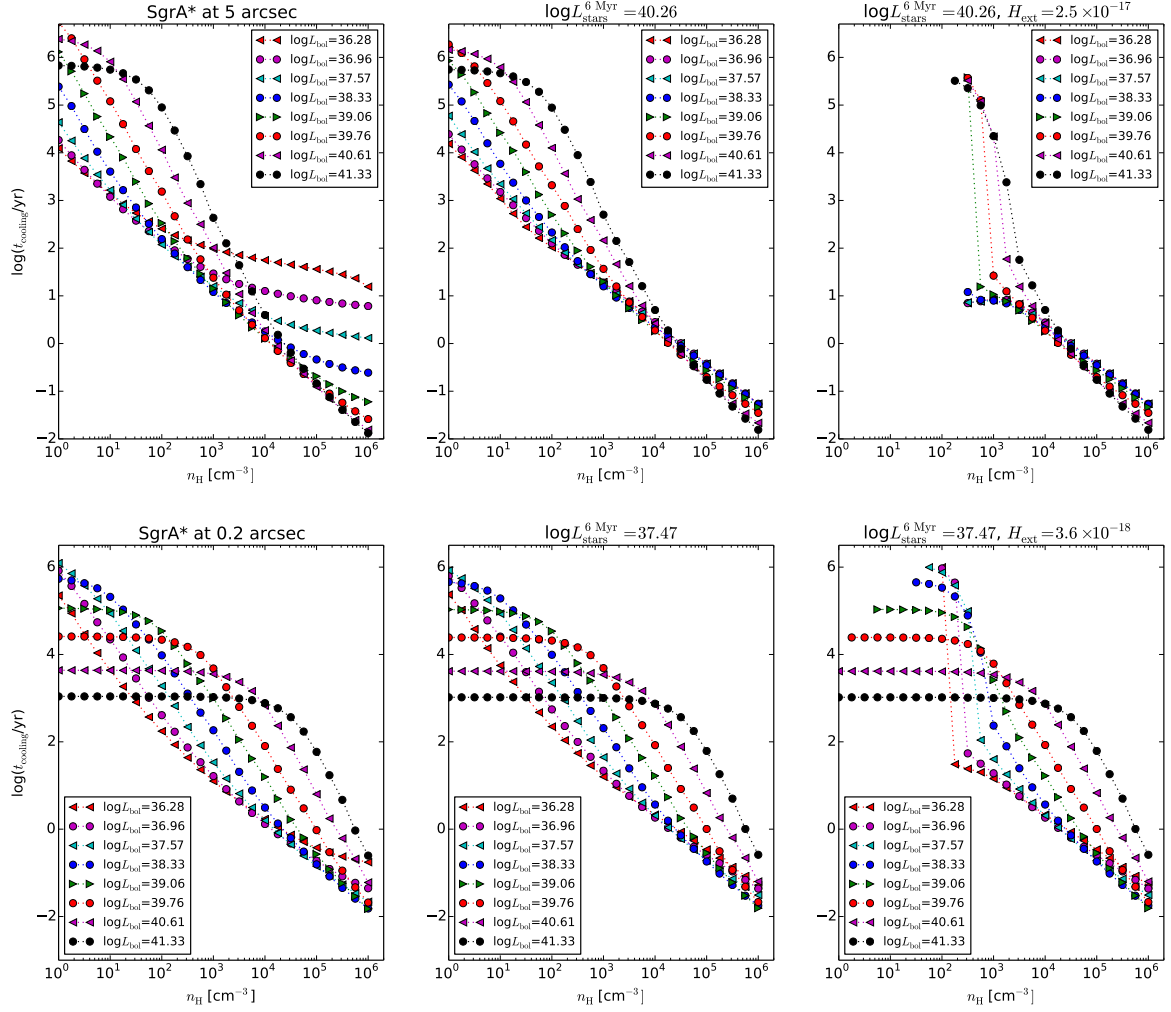


Figure 3. Equilibrium cooling timescale in the case of Sgr A* for different luminosity states of the radiation: from the central source only (left panels), together with heating by stellar radiation (middle panels), and together with mechanical heating by winds (right panels). The results presented here are for the same model parameters as in Fig. 2.

parameter: $\Xi = L_{\text{stars}}/(4\pi c P_{\text{gas}} R^2)$ is the same, iv) by changing input parameters for CLOUDY, which means that to keep the ionization parameter the same, and for the same density, changing the distance (for Sgr A*, from 0.2 arcsec to 5 arcsec) requires changing the input L_{stars} . The appropriate values of stellar luminosities are always listed in the figures.

The “mechanical” heating by stars is described following the approach of Shcherbakov & Baganoff (2010). As in their Fig. 3, we adopted values for the stellar mass input into the feeding region around BH equal to $10^{-8} M_{\odot} \text{yr}^{-1}$ and wind velocity 1000 km s^{-1} at a distance of 0.2 arcsec from the nucleus. The mass input at a distance of 5 arcsec is $3 \times 10^{-5} M_{\odot} \text{yr}^{-1}$, and the wind velocity equals 1200 km s^{-1} . This leads to a mechanical heat input of

$$H_{\text{ext}} = \begin{cases} 3.6 \times 10^{-18} [\text{erg s}^{-1} \text{cm}^{-3}] & \text{at } r = 0.2 \text{ arcsec,} \\ 2.5 \times 10^{-17} [\text{erg s}^{-1} \text{cm}^{-3}] & \text{at } r = 5 \text{ arcsec.} \end{cases} \quad (8)$$

The description of the heating in the inner region is a crude approximation, since it relies on a single star being present in this region. As in Shcherbakov & Baganoff (2010), we neglect here the

velocity of the star itself, as the fate of the lost material is an open issue. The velocity of this star is likely higher (the Keplerian velocity at a radius of 0.008 pc is 1500 km s^{-1} for a $4 \times 10^6 M_{\odot}$) than the wind velocity (assumed to be 1000 km s^{-1} here). Such a wind is partially focused in the direction of the stellar motion. So on one hand we should assume that the effective velocity of the wind is enhanced due to the stellar velocity, but on the other hand part of the material may leave the region as a stream and not dissipate all the energy in situ. Since the wind mass loss is provided as an order of magnitude estimate, we do not include the stellar motion into the heating term.

As mentioned above, we study the thermal equilibrium conditions around Sgr A* at two representative radii, 5.0 and 0.2 arcsec, corresponding to a linear distance of about 0.2 pc and 0.008 pc from the center, respectively. The stability curve is obtained by running a grid of CLOUDY simulations for constant hydrogen number density clouds spanning a range from $\log n_{\text{H}} = 0$ up to $\log n_{\text{H}} = 6.25$. The results for both distances are shown in Fig. 2 (upper and lower panels respectively). The left panels show the results when only radiative heating by the accreting material affects the ionization equi-

librium. The present level activity of Sgr A* is too low to support a high temperature of the medium, and only the cold equilibrium branch exists. A higher level of activity in the past, however, could have heated the plasma up to the Inverse Compton temperature, i.e. $T \sim 10^8$ K.

The addition of stellar light (middle panels in Fig. 2) to radiative heating by the central source results in a decrease of temperature of the irradiated medium. Stellar light thus effectively cools the gas even though the stars are blue and young. Since the central emission has a strong X-ray component, the addition of a blue light provides additional soft photons, which lowers the Inverse Compton temperature of the incident radiation.

We have checked that higher metallicities in the stellar population does not change our results. The SED of high metallicity stars is not very different from the solar case (see Fig. 1), and the resulting plots for the S-curves did not show any noticeable differences in comparison to Fig. 2. Also the contribution of an older stellar population of 1 Gyr stars does not change quantitatively the location of TI presented in Fig. 2 since those stars are two orders of magnitude less luminous (despite their larger total mass). But the inclusion of mechanical heating by stellar winds changes the picture dramatically. We demonstrate this in the right panels of Fig. 2. Although we were not able to cover the entire low-density range for the case of high-luminosity and large distance, even for the displayed span of density the equilibrium temperatures exhibit unrealistically extreme values. Cold clumps can exist in thermal equilibrium but they must be very dense. Closer to the black hole the stellar mechanical heating is one order of magnitude lower, the radiative effects are of greater importance, and we still have the upper stable branch of solution at the Inverse Compton temperature for the highest luminosity states. Again, an increase in metallicity of the stellar population or the inclusion of an additional older population of stars, do not change our results.

The present-day activity level of Sgr A* supports temperatures up to 10^5 K on the stable branch but only for densities higher than $n_H \sim 10^2 \text{ cm}^{-3}$ (e.g., Wang et al. 2013; Róžańska et al. 2015, and further references therein). Lower-density gas gets heated to a much higher temperature even at a small distance from the black hole. The time taken for the low-temperature phase to reach equilibrium is long. In Fig. 3 we show the cooling timescales for plasma in equilibrium: for densities lower than 10^2 cm^{-3} the cooling timescales exceed 10^4 yr.

This has to be compared with the characteristic timescale of inflow and outflow. The stagnation radius, dividing the inflow from outflow in Sgr A*, is currently located between 0.3 to 1 arcsec (Quataert 2004; Shcherbakov & Baganoff 2010). Thus our solution at 0.2 arcsec is within the accretion flow part. The inflow proceeds initially with a velocity which is a small fraction of the stellar wind velocity (zero speed formally at the stagnation radius). Assuming that the inflow velocity is 10% of the of the stellar wind velocity, i.e. ~ 100 km/s, we obtain an infall timescale of 100 yr, much shorter than the cooling timescale. Thus, close to the nucleus of Sgr A*, the adiabatic picture of the hot plasma as presented by Quataert (2004) is satisfactory. However, if cold, sufficiently dense clumps of gas happen to arrive in that region from outside they will also survive due to the presence of the cold equilibrium branch.

The solution at 5 arcsec is in the outflow part, above the stagnation radius. The outflow proceeds predominantly with a speed comparable to the wind speed. Again, we see that there is no time for a low density plasma to cool down unless the outflow finally stops due to collision with the outer ambient medium that is initially far from thermal equilibrium.

Stars supply a moderately hot, $T \sim 10^6$ K, low-density material. This temperature does not coincide with the equilibrium solution (see Fig. 2) and the plasma may remain away from the thermal equilibrium curve since the timescales for reaching thermal balance are long (see Fig. 3). We thus address separately the issue of thermal evolution of this freshly injected plasma.

For this, we fix the plasma temperature at 10^6 K and calculate the cooling timescale as a function of density, at both representative radii, 5 and 0.2 arcsec. The results are shown in Figs. 4 and 5, respectively. The upper panels show timescales computed with Eq. (6) assuming the total heating given as an output in `CLOUDY` computations, middle panels show the same for cooling only, and the bottom panels show ratios of those two values. The cooling timescales for a very dense plasma are relatively short in comparison to the heating timescales. Therefore, we conclude that for densities higher than $\sim 10^3 \text{ cm}^{-3}$, cooling dominates over heating. Recent X-ray observations of hot plasma in the vicinity of Sgr A* indicate that the plasma density is of the order of $10\text{--}100 \text{ cm}^{-3}$ (Shcherbakov & Baganoff 2010; Róžańska et al. 2015), and for such low densities heating dominates. The timescales are short, of the order of 100 years, and in the case of the smaller radii (Fig. 5), they significantly depend on the actual luminosity state of Sgr A*. Therefore, vigorous hot plasma outflow is expected from most of the region, both at the present level of moderate Sgr A* activity and in the past. Occasional strong wind collisions may result in some local plasma compression and formation of clouds but the requested compression factor is large, so the phenomenon is unlikely to be frequent.

Spontaneous formation of cold clouds from the low density medium is not expected. On the other hand, in the GC mini-spiral region numerous cold dense clouds do exist, as an intense IR emission from that region is observed (Becklin et al. 1978; Gezari et al. 1985). We thus repeated a similar non-equilibrium study as above, but for clouds with temperatures of 1.4×10^4 K, determined observationally from the mini-spiral. As in the previous two figures, heating and cooling timescales for matter located at 5 and 0.2 arcsec from the center are presented in Figs. 6 and 7 respectively. We see that clouds denser than 10^4 cm^{-3} reach equilibrium in timescales shorter than 100 years and preserve it. Such clouds are thus located in the lower part of the equilibrium curve. They will be surrounded by a rapidly expanding/outflowing hot phase. The interaction of colder clouds with the hot medium may finally lead to cloud destruction but this issue is far beyond the scope of this paper, as the phenomenon will likely depend on the actual cloud motion, and likely also on the magnetic field intensity. Computations presented in this paper only show that the cold medium phase of the mini-spiral is not produced 'in situ' and had to form in a different way than due to thermal instability in the hot plasma heated by radiation and stellar winds.

3.2 Case of M60-UCD1

Ultra-Compact Dwarf galaxies, apart from the characteristic compact size of their dense nuclear stellar cluster generally exhibit elevated mass-to-light ratios (Fellhauer & Kroupa 2006; Mieske 2014). M60-UCD1 is an exceptional example with tentative evidence, based on stellar kinematics, for a supermassive black hole in the core (Strader et al. 2013; Seth et al. 2014; Reines 2014). The object has also been detected as a variable X-ray source (Luo et al. 2013). We can thus apply to this source a similar analysis as in the previous section.

In the first step we again construct a model of the broad-band

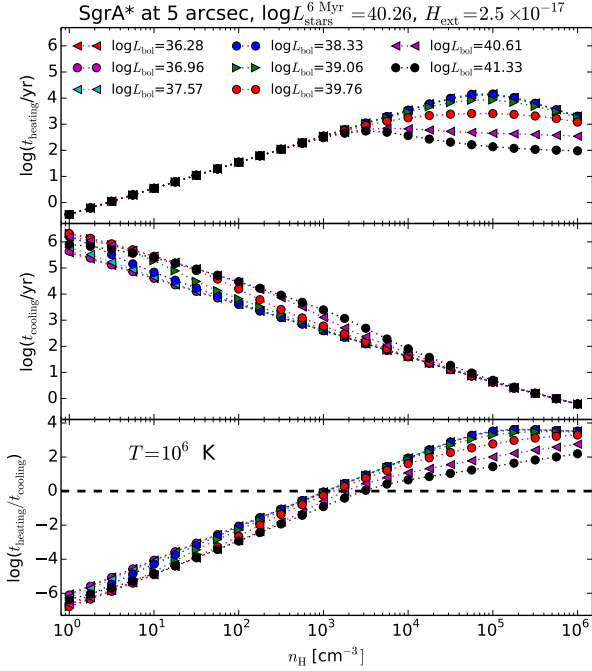


Figure 4. Sgr A* heating (upper panel) and cooling (middle panel) time-scales plotted against cloud density. Bottom panel represents ratio of those two values. The ISM gas in each case is heated by radiation from the center with different luminosity states, radiation from stars $\log(L_{\text{stars}}/\text{erg s}^{-1}) = 40.03$, and volume mechanical heating $H_{\text{ext}} = 2.5 \times 10^{-17} \text{ erg s}^{-1} \text{ cm}^{-3}$. Each cloud is assumed to have a temperature of $T = 10^6 \text{ K}$ and is located at an offset of 5 arcsec from the center.

spectrum emitted from the accretion inflow from Mościbrodzka et al. (2012). But in case of M60-UCD1, the X-ray luminosity between 2–10 keV is $1.3 \times 10^{38} \text{ erg s}^{-1}$ (Strader et al. 2013), i.e., higher than in Sgr A*. Therefore, we re-scale the broad-band spectra used in the Sgr A* calculations to obtain the observed value of the X-ray luminosity between 2–10 keV for this source. All eight different luminosity states used in our photoionization calculations are presented in Fig. 8. In the second step we model the stellar emission of M60-UCD1 nuclear star cluster with STARLIGHT (Cid Fernandes et al. 2011), taking the total mass of the stars to be $1.2 \times 10^8 M_{\odot}$ (Seth et al. 2014) and assuming the age of the stars to be 13 Gyr (Strader et al. 2013). The SED from stars used in cloudy computations is presented in Fig. 1 as black dots.

Stars in M60-UCD1 are much older than stars in the Sgr A* neighborhood, so they are not sources of vigorous winds. Main sequence stars of the age of the Sun are sources of fast winds. The solar wind has a wind outflow rate of $\sim 10^{12} \text{ g s}^{-1}$, and an outflow velocity $\sim 500 \text{ km s}^{-1}$. If we assume that all the stars are in this form and that they uniformly occupy the core within a radius of 24 pc, we arrive at a main sequence stellar mass loss of $3 \times 10^{-6} M_{\odot} \text{ yr}^{-1}$ and their contribution to the total heating

$$H_{\text{MS}} = 1.0 \times 10^{-25} \text{ erg s}^{-1} \text{ cm}^{-3} \text{ for } r < 24 \text{ pc.} \quad (9)$$

Most of the mass loss, however, happens at the post main sequence stage. There, the mass loss is driven by the presence of dust in the stellar envelope. The total mass loss of a single star is of order of $10^{-6} M_{\odot} \text{ yr}^{-1}$, but the strong wind stage is short, and the wind ve-

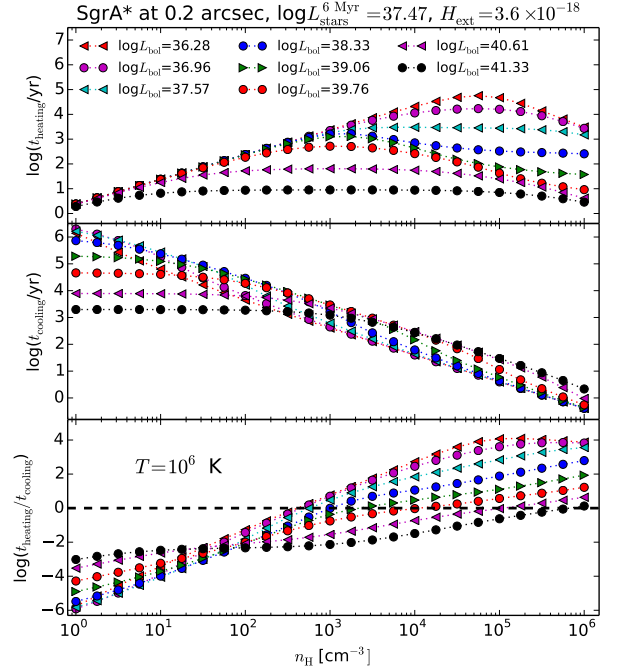


Figure 5. Sgr A* heating (upper panel) and cooling (middle panel) time-scales plotted against cloud density. Bottom panel represents ratio of those two values. The ISM gas in each case is heated by radiation from the center with different luminosity states, radiation from stars $\log(L_{\text{stars}}) = 37.47 \text{ erg s}^{-1}$, and volume mechanical heating $H_{\text{ext}} = 3.6 \times 10^{-18} \text{ erg s}^{-1} \text{ cm}^{-3}$. Each cloud is assumed to have a temperature of $T = 10^6 \text{ K}$ and is located at a distance of 0.2 arcsec from the center.

locity is small, of order of 10 km s^{-1} . This velocity is much smaller than the stellar velocity dispersion in UCD1 (70 km s^{-1} , Strader et al. 2013). The effective mass loss from the entire stellar population has been estimated to be $2.5 \times 10^{-12} M_{\odot} \text{ yr}^{-1} M_{\odot}^{-1}$, under the assumption of a Salpeter mass distribution (Pellegrini 2012). Taking this mass loss, and the dispersion velocity instead of the wind velocity we obtain the total heating

$$H_{\text{PMS}} = 7.0 \times 10^{-25} \text{ erg s}^{-1} \text{ cm}^{-3} \text{ for } r < 24 \text{ pc.} \quad (10)$$

Although supernova eruptions in such a small and old stellar population are rare, their average contribution is important. Assuming the intrinsic B band luminosity $6 \times 10^5 L_{\odot}$ and using Eq. 3 of Pellegrini (2012), we obtain the mean energy deposition per unit volume

$$H_{\text{SN}} = 2.7 \times 10^{-24} \text{ erg s}^{-1} \text{ cm}^{-3} \text{ for } r < 24 \text{ pc.} \quad (11)$$

We take the sum of the contributions from the three stellar heating channels as the final stellar heating rate:

$$H_{\text{ext}} = 3.1 \times 10^{-24} \text{ erg s}^{-1} \text{ cm}^{-3} \text{ for } r < 24 \text{ pc.} \quad (12)$$

This is more than 6 orders of magnitude lower than for Sgr A* but comparable to various heating processes operating in the disk of the Milky Way galaxy (Klessen & Glover 2016).

We calculate the thermal equilibrium curves at two distances from the centre, i.e. at 24 pc (which is the half-light radius of the NSC), and further inside at 0.2 pc. The gas is expected to be less dense, therefore we consider clouds spanning the range from

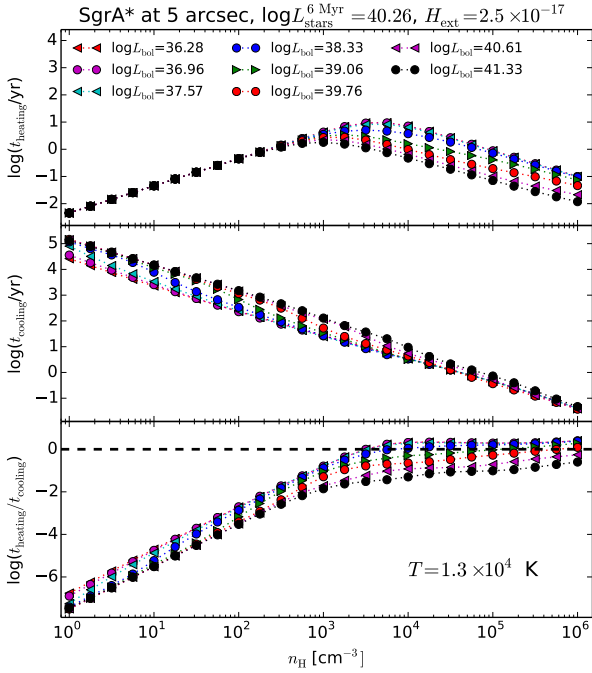


Figure 6. The same as in Fig. 4 but each cloud is assumed to have temperature $T = 1.3 \times 10^4$ K.

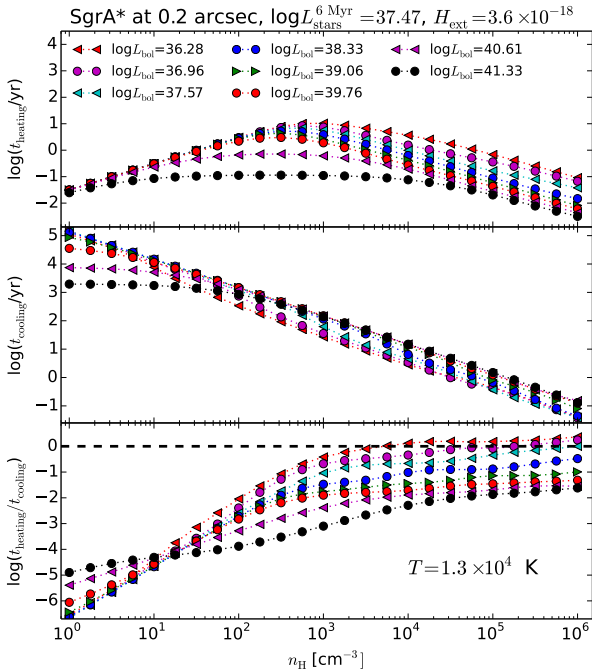


Figure 7. The same as in Fig. 5 but each cloud is assumed to have temperature $T = 1.3 \times 10^4$ K.

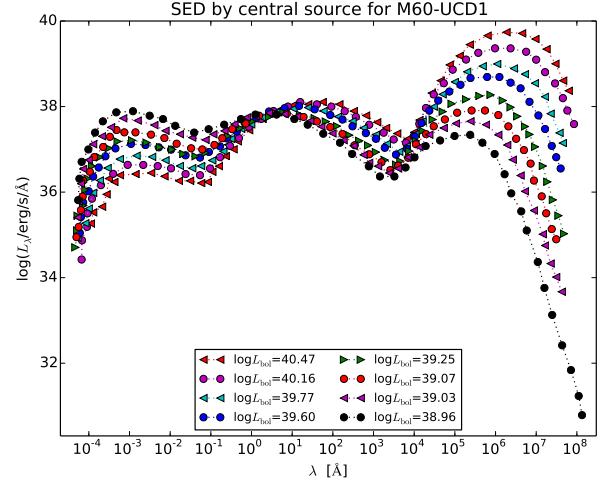


Figure 8. The M60-UCD1 broad-band continuum assumed in the computations. The shape of different luminosity states for Sgr A* is normalized to take into account the observational value of the X-ray flux for M60-UCD1: $L_X(2-10 \text{ keV}) = 1.3 \times 10^{38} \text{ erg/s}$.

$\log n_H = -3$ up to $\log n_H = 2.5$. The results for both distances are shown in Fig. 9 upper and lower panels, respectively. The upper panels clearly show that the distance of 24 pc from the center is far enough to prevent matter from being strongly ionized. The radiation is not hard enough to heat up the gas to the high equilibrium branch. High (unrealistic) temperatures appear for very low densities (below 0.03 cm^{-3}) only when mechanical heating is included (right panel). However at a distance of 0.2 pc from the center, the radiation field from the accreting gas is hard enough for the high temperature branch to appear. Soft photons from old stars cool down this gas, which is clearly shown in the middle bottom panel. Finally, closer to the center mechanical heating is not able to heat the gas to such unrealistically high temperatures.

The thermal timescales for the plasma in equilibrium are shown in Fig. 10. The timescales are shorter for the cold dense gas, but they are still quite long, of the order of 10^7 yr, for the low density high temperature plasma located at 0.2 pc. In the case when mechanical heating dominates in the gas at the distance of 24 pc, the cooling timescale for low density plasma can reach 10^{10} yr.

We can estimate the mean density of the hot phase originating from the thermalized stellar winds as the basis of the observed X-ray emission ($L_X = 1.3 \times 10^{38} \text{ erg s}^{-1}$), assuming this emission is predominantly due to bremsstrahlung. We adopt a stellar wind temperature, $T_{\text{wind}} = 10^6 \text{ K}$. Assuming the size of the emitting region to be the nuclear radii, we have

$$n_{\text{mean}} = 7.32 \times \left(\frac{T}{10^6 \text{ K}} \right)^{-1/4} \text{ cm}^{-3}. \quad (13)$$

For these densities, the timescales in equilibrium are quite short, 10^3 yr, and the plasma moves toward the equilibrium curve shown in Fig. 9. However, at this density and temperature the plasma is not in local thermal equilibrium, as can be seen from the equilibrium curve. The cooling dominates, since the mean bremsstrahlung emission is of order of $7.64 \times 10^{-23} \text{ erg s}^{-1} \text{ cm}^{-3}$ (i.e. almost two orders of magnitude higher than the heat input from stellar winds). Therefore, we perform computations of the cooling timescale for a fixed temperature and a range of densities to see the trend in the plasma far from thermal equilibrium. Plasma produced from stel-

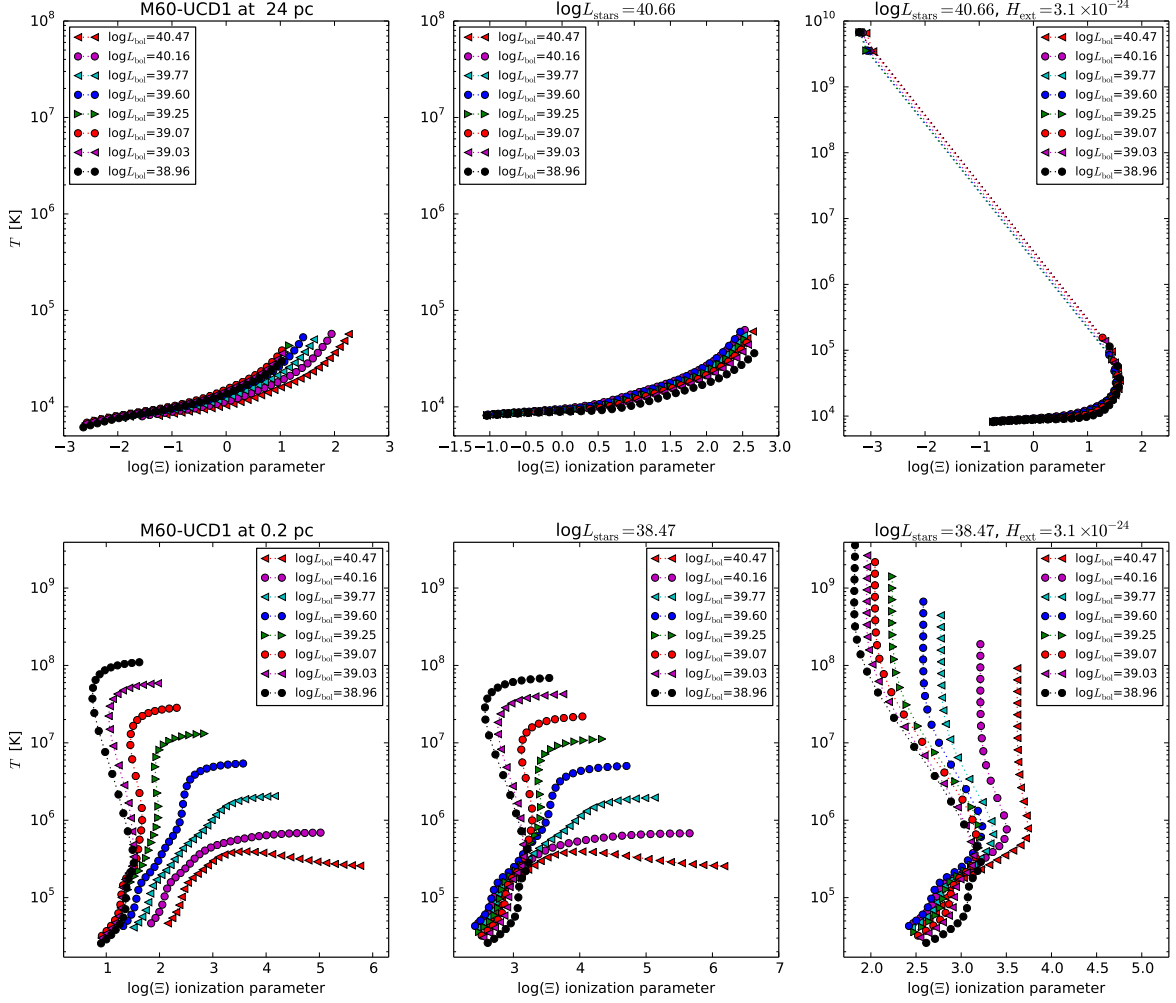


Figure 9. Solutions for S-curve of TI in the plane of temperature vs. ionization parameter, as defined in Eq. 5, in case of M60-UCD1, for different luminosity states of the radiation: from the central source only (left panels), together with heating by stellar radiation (middle panels), and together with mechanical heating by winds (right panels). Values of central source luminosity are marked within the panels. We present results for the gas located at 24 pc from M60-UCD1 (upper row of panels) and at 0.2 pc (bottom row of panels). The luminosity of the NSC is equal to $\log(L_{\text{stars}}/\text{erg s}^{-1}) = 40.66$ at 24 pc and $\log(L_{\text{stars}}/\text{erg s}^{-1}) = 38.47$ at 0.2 pc, and the volume mechanical heating is always $H_{\text{ext}} = 3.1 \times 10^{-24} \text{ erg s}^{-1} \text{ cm}^{-3}$.

lar winds cools down if the density is higher than 0.1 cm^{-3} (see Fig. 11), and at the mean density estimated above it needs $\sim 10^4 \text{ yr}$ to cool down.

If the star is close to the edge of the nucleus and the outflow velocity is of the same order as the wind velocity, the plasma may leave the nucleus before it cools significantly. The crossing time is only

$$t_{\text{cross}} = 4.7 \times 10^4 [\text{yr}]. \quad (14)$$

The plasma in outer parts of the nucleus thus preserves the energy content formed in the stellar wind interactions. An adiabatic description offers an acceptable approximation although cooling is not completely negligible.

However, if the star is located close to the stagnation point between the outflow and inflow, then the velocity is much lower, the plasma can cool down and form colder and denser clumps (see Quataert 2004; Shcherbakov & Baganoff 2010, for a discussion in the context of Sgr A*).

The stagnation radius, R_{st} , for M60-UCD1 can be estimated using the formula (Silich et al. 2008)

$$R_{\text{st}} = \left(\frac{GM_{\bullet}}{2R_{\text{NSC}}v_{\text{A}\infty}^2} \right)^{2/3} R_{\text{NSC}}, \quad (15)$$

where R_{NSC} is the NSC (half-light) radius, and $v_{\text{A}\infty}$ is the terminal velocity of the stellar wind. Here we neglected dimensionless coefficients which depend on the polytropic index. Assuming a terminal velocity three times higher than the wind velocity (i.e. 1500 km s^{-1}) we obtain $R_{\text{st}} = 0.01 R_{\text{NSC}}$, deep inside the NSC. Most of the material thus starts to flow out. The radiative cooling is then partially assisted by the adiabatic cooling. The cooling timescale is an order of magnitude longer than in the outskirts of the galaxy (see Fig. 13) but the cooling still dominates and adiabatic expansion will assist this trend. Therefore, spontaneous cloud formation is likely, although time-dependent modeling coupled with the inflow/outflow dynamics would be necessary to confirm this trend.

This picture is strongly different from the situation in Sgr A*,

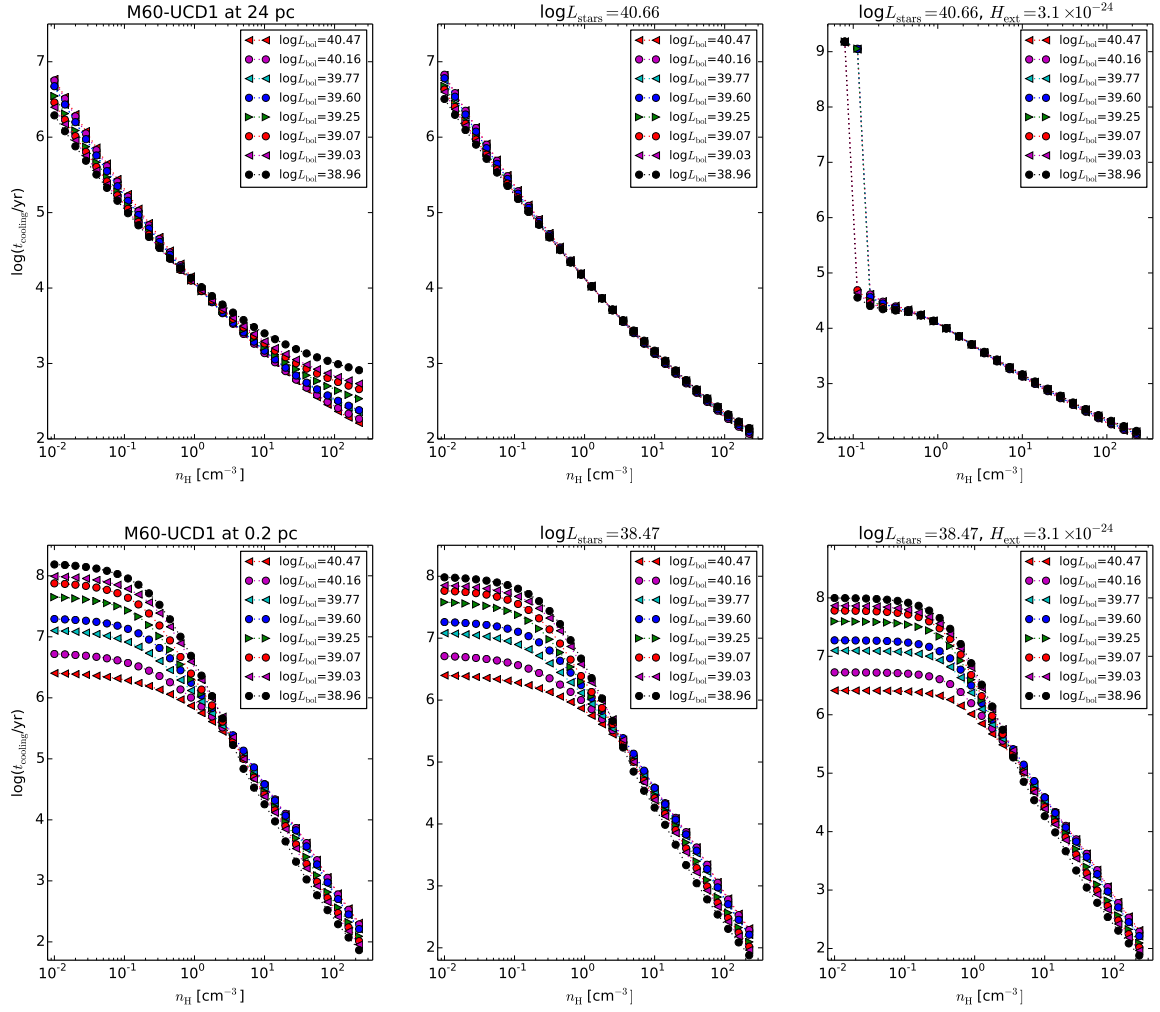


Figure 10. Equilibrium cooling timescale in case of M60-UCD1, for different luminosity states of the radiation: from the central source only (left panels), together with heating by stellar radiation (middle panels), and together with mechanical heating by winds (right panels). The results presented here are for the same model parameters as in Fig. 10.

where the locally inserted stellar wind cannot cool down due to the stellar heating always dominating the radiative cooling inside the inner parsec.

4 DISCUSSION

We considered the thermal stability of plasma in the innermost regions of compact stellar clusters surrounding a supermassive black hole. We discussed in particular two cases: the nuclear cluster in the Milky Way and the Ultra-Compact Dwarf galaxy M60-UCD1. We found that the conditions are more extreme in the case of Sgr A* due to the higher compactness of the nuclear cluster: stellar heating prevents the spontaneous formation of cold clouds out of the freshly inserted stellar wind plasma. On the other hand, if cold dense clumps of material happen to be in this region, they can stay in thermal equilibrium. From observations, the existence of cold plasma in the mini-spiral region is well known which is consistent with our scenario but the origin of that plasma is then clearly non-local. Fresh plasma from stellar winds joins the hot X-ray emitting

phase seen in X-ray images and it forms an outflow, as modeled by Quataert (2004) and Shcherbakov & Baganoff (2010).

In the case of M60-UCD1 mechanical heating by stellar winds is not as intense and we expect spontaneous formation of cold clouds in the inner part of the galaxy, close to the stagnation radius, since the cooling timescales are then shorter than the inflow/outflow timescale. Let us note that our paper addresses only the direction of time evolution in case of a thermal imbalance in the medium, leaving aside the dynamical interaction of the cold clouds with the hot surrounding medium.

A complete non-stationary picture of the behavior of the multi-phase medium can be obtained only by three-dimensional time-dependent numerical computations. The main advantage of the numerical approach is obviously the consistency of the description and the possibility to include additional effects. On the other hand, a large number of free parameters complicates the interpretation, and so both the numerical and semi-analytical approaches are useful and complement each other.

It is interesting to note that, recently, Barai et al. (2012) have shown that cooler clumps form filaments near a SMBH, which then

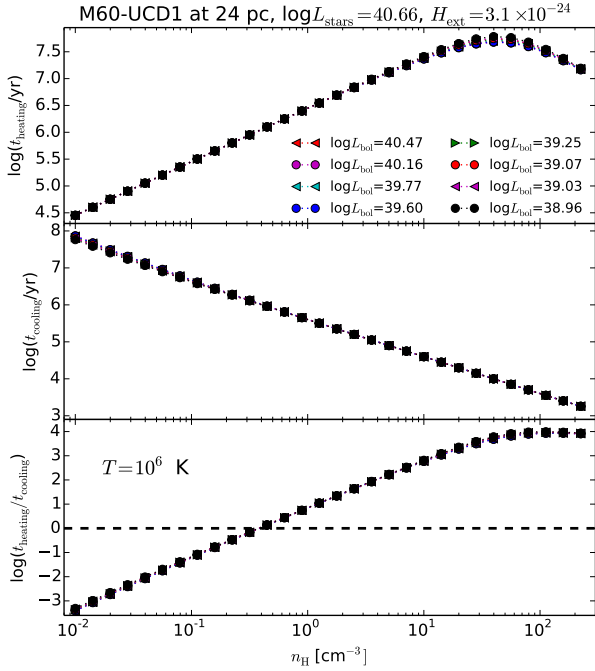


Figure 11. M60-UCD1 heating (upper panel) and cooling (middle panel) time-scales plotted against cloud density. Bottom panel represents ratio of those two values. The ISM gas in each case is heated by radiation from the center with different luminosity states, radiation from stars of $\log(L_{\text{stars}}/\text{erg s}^{-1}) = 40.66$, and volume mechanical heating $H_{\text{ext}} = 8.8 \times 10^{-26} \text{ erg s}^{-1} \text{ cm}^{-3}$. Each cloud is assumed to have a temperature $T = 10^6 \text{ K}$ and is located at a distance of 24 pc from the center.

accrete faster than the surrounding hot plasma. Hueyotl-Zahuantitla et al. (2013) studied the evolution of matter reinserted by stars in a rotating young NSC. These authors employed a hydrodynamic model that includes gravitational attraction from the central SMBH and NSC, and it also takes radiative cooling and heating from the central source into account. By following the formation of thermally unstable zones for a large set of parameters of the NSC and SMBH, including those relevant for the present state of the Galactic centre, Hueyotl-Zahuantitla et al. (2013) concluded that for a NSC of mass $3.3 \times 10^7 M_{\odot}$ and size 10 pc, SMBH mass $M_{\bullet} \approx 1 \times 10^6 M_{\odot}$ and accretion luminosity $L \approx 1.3 \times 10^{38} \text{ ergs s}^{-1}$, the central source of radiation heats the gas up to a few $\times 10^7 \text{ K}$. This prevents the development of the Thermal Instability.

In the context of galaxy outflows, Scannapieco & Brüggen (2015) have recently performed numerical simulations of the evolution of cold clumps embedded in an outflowing medium. Their results show that clouds can survive within a supersonic flow for a period of time long enough to be accelerated by the flow, although the outflowing clouds are gradually destroyed. In our model we consider a close region above and below the stagnation radius, and so the orientation of the radial motion can be directed with either positive or negative radial velocity component, depending on the interplay of hydrodynamic friction by the ambient medium, radiation pressure from stars in the NSC, and the gravitational attraction of the SMBH.

In our considerations we assumed that the electrons and ions are well coupled and form a single-temperature plasma. This is jus-

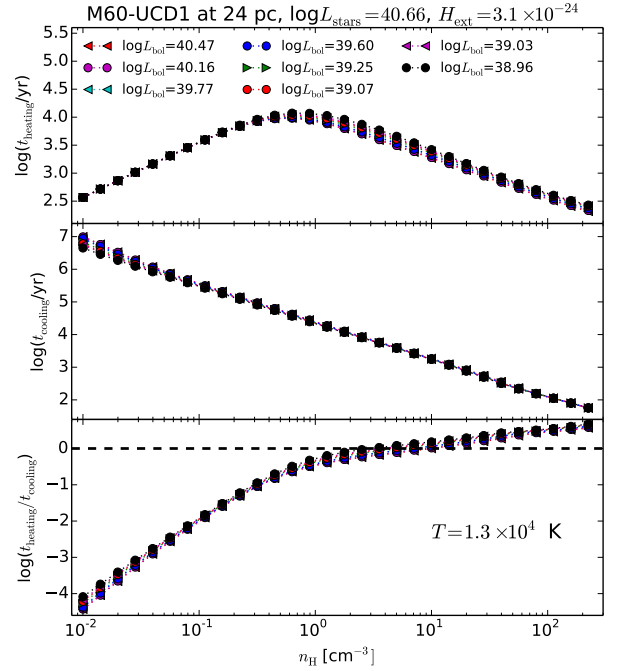


Figure 12. The same as in Fig. 11 but each cloud is assumed to have temperature $T = 1.3 \times 10^4 \text{ K}$.

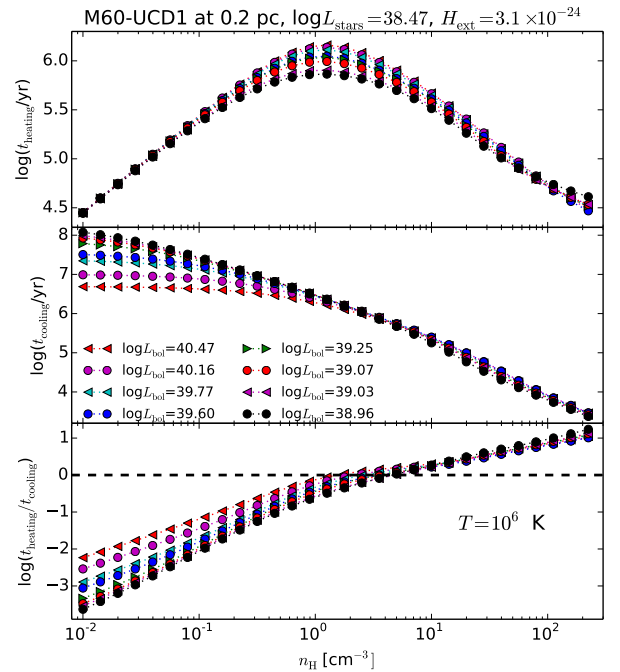


Figure 13. The same as in Fig. 11 but for gas located at 0.2 pc from the M60-UCD1 center.

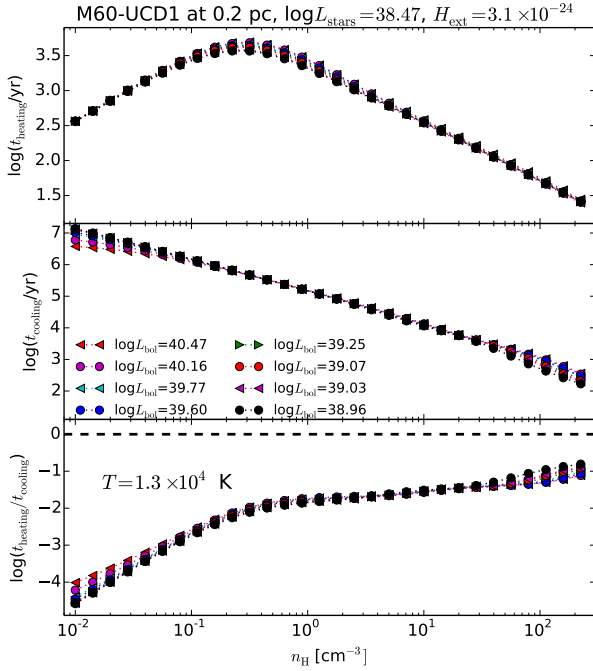


Figure 14. The same as in Fig. 13 but each cloud is assumed to have temperature $T = 1.3 \times 10^4$ K.

tified since several studies of spherical hot accretion onto Galactic Center show that a two-temperature plasma develops only within the innermost tens of gravitational radii (<0.1 arcsec) from the black hole (Moscibrodzka 2006; Mościbrodzka et al. 2009; Shcherbakov et al. 2014). In addition, strong arguments in favour of very efficient electron-ion coupling (Bisnovatyi-Kogan & Lovelace 1997) imply that this region is very small.

We have not yet included the role of magnetic fields in our scheme but we note that they are important for TI, although this issue is difficult to explore due to the enormous richness of possible configurations. Already in his seminal paper, Field (1965) realized that magnetic fields penetrate the interstellar plasma and influence the onset of TI. First, the internal pressure gets increased by the magnetic term which must be added to the gas pressure (Langer 1978). This is, however, a rather minor and mainly quantitative change under usual conditions of the interstellar medium, unless the magnetic field exceeds the equipartition value ($P_m \gtrsim P_g$). This may be the case very close to the horizon, where Sgr A* flares are thought to occur. A more important mechanism is anisotropic transfer of heat across the field lines, for which the presence of a magnetic field of relatively weak (sub-equipartition, $P_m \ll P_g$) intensity is sufficient. This is caused by the fact that the motion of electrons is greatly reduced in the direction across the field lines. However, in the plane-parallel approximation the growth timescale of the condensation instability is not diminished very strongly, unless the magnetic field is strictly perpendicular to the temperature gradient (van Hoven & Mok 1984).

Celotti & Rees (1999) studied the possibility that cold material may be confined by the ambient magnetic field that pervades the hot medium, thereby establishing conditions for co-existence of phases at very different temperature. These authors considered

a quasi-equipartition case when the magnetic pressure approximately equals the gas term. According to their scenario the main role of the magnetic field is to trap plasma in clouds that have enough time to cool down to the Compton temperature. Quite recently, Wang et al. (2012) explored the velocity dispersion of cold clouds embedded in an advection dominated accretion flow (ADAF), and Khajenabi & Rahmani (2015) also included the effect of weak (sub-equipartition) magnetic fields. While the cold phase can naturally attain the form of localized clouds, one-dimensional (filamentary) structures have also been suggested.

The role of magnetically induced anisotropy depends critically on the magnetic field structure (the tangled small-scale magnetic loops vs. large-scale organized field lines) and the ionization state of the medium (hot, fully ionized plasma is more sensitive to the imposed magnetization than the cooler medium with only partial degree of ionization). Burkert & Lin (2000) found that tangled magnetic fields reduce the conductive heat flux. As a result, low-amplitude fluctuations can grow until the nonlinear effects start operating at length-scales of order ~ 0.01 pc. Magnetization enhances the filamentary structures, which are inherently three-dimensional and their discussion requires numerical approaches (Parrish et al. 2009; McCourt et al. 2012; Sharma et al. 2012).

Thus, while the additional mechanical heating from stellar winds tends to suppress the Thermal Instability, magnetic fields effectively insulate the gas elements in the direction perpendicular to the field lines, thereby decreasing the heat conduction and permitting large temperature gradients across the field lines. As a consequence, the multi-phase structure is maintained. Nonetheless, the magnetic structure and the source of heating are critical but largely unknown.

Tenorio-Tagle et al. (2013) studied gas and dust cooling in centers of young, massive, compact star clusters (typical length-scales of ~ 10 pc). Interestingly, TI operates and an unstable region develops also in these systems. Based on STARBURST99 (Leitherer et al. 1999) synthesis computations we find that matter reinserted in the thermally unstable volume is reprocessed into dense clouds and there it leads to a new phase of star formation.² Very recently, Dale (2015) reviewed the operation of TI in the context of state-of-art numerical simulations of the multi-phase environment in stellar systems with feedback. In fact, the physical origin of feedback processes in stellar systems is analogous to the widely discussed feedback mechanism in active galactic nuclei (Fabian 2012), although the scales and conditions are vastly different. An important message from these studies is the recognition of the fact that these systems behave in a self-regulating regime for which an accurate description of cooling and heating processes is essential.

Additional mechanisms contribute to the feedback processes and may eventually enhance the mechanical heating above the level assumed in our simplified scenario, but only some of them can be relevant in evolved stellar systems (Ciotti & Ostriker 2007; Pellegrini et al. 2012). In particular, after a star-forming burst at a certain moment, the mass and energy injection from massive stars peak at earlier time with respect to the input from the post-main-sequence population, and from supernovae Type II explosions.

² Let us note that, similarly to our analysis in the previous section but without the central black hole, Tenorio-Tagle et al. (2013) found that only a limited fraction of the released mechanical energy from stars is transferred back into the ISM.

5 CONCLUSIONS

We studied the conditions for the onset of the Thermal Instability in compact stellar systems with a supermassive black hole residing in the core. As the Thermal Instability develops, it can help cold clumps to survive in the surrounding hot medium and drive them toward the central SMBH, thus enhancing the mass accretion rate during episodes of clumps disruption and inflow.

The Nuclear Star Cluster in the centre of the Milky Way and the Ultra-Compact Dwarf galaxy UCD1 near M60 galaxy represent prototypical systems with a small half-light radius and large mass-to-light ratio, suggesting that an interplay between gravitational, radiative, and hydrodynamic influences leads to an interesting richness of the evolutionary tracks of the accreting SMBH. A large number of UCDs have been discovered in the last decade, however the presence of SMBHs at the centres of UCDs remains an open question. Sgr A* is the best-resolved extreme example of a galactic nucleus with a Nuclear Star Cluster in addition to a SMBH.

To explore the possibility of TI as a driver that triggers variability via accretion episodes, we discussed an appropriate definition of the ionization parameter Ξ and studied the position of different systems with respect to the S-curve in the instability diagram. In addition to the effect of X-ray irradiation from the core we also took the cooling effect of ambient stellar radiation and mechanical heating from colliding winds into account, and we considered the presence of stagnation radius R_{st} in the Bondi-like hot inflow/outflow. We showed that Thermal Instability indeed operates under suitable conditions while it can be suppressed in other parts of the parameter space during the evolution of the system. Cold clouds can thus remain within the surrounding hot diluted medium for a relatively long period.

A more complete multi-wavelength picture of these systems can help to constrain the state of their ISM in the future. Current evidence for the presence of a SMBH at the centre of M60-UCD1 arises from dynamical modeling of adaptive optics kinematic data (Seth et al. 2014). However, apart from a tentative detection in X-rays, there is very little information about the SED of the central black hole. As we have seen in Section 3.2, the shape of the SED of the central black hole influences the formation of TI close to the SMBH. Follow-up observations in the X-ray and radio continuum can help to detect signatures of accretion in the central black hole and provide a more realistic SED. Observations in the infrared can also reveal the presence of dust/gas in the central regions to get a better estimate of the properties of the ISM in those objects.

ACKNOWLEDGMENTS

This research was supported by Polish National Science Center grants No. 2011/03/B/ST9/03281, 2013/10/M/ST9/00729, 2015/17/B/ST9/03422, 2015/18/M/ST9/00541 and by Ministry of Science and Higher Education grant W30/7.PR/2013. We also received funding from the European Union Seventh Framework Program (FP7/2007-2013) under grant agreement No. 312789, and Czech Science Foundation “Albert Einstein Center for Gravitation and Astrophysics” (GAČR 14-37086G). We acknowledge the Czech Ministry of Education, Youth and Sports COST project LD15061 titled “Astrophysics of toroidal fluid structures around compact stars”.

References

- Barai P., Proga D., Nagamine K., 2012, *MNRAS*, **424**, 728
- Becklin E. E., Matthews K., Neugebauer G., Willner S. P., 1978, *ApJ*, **219**, 121
- Begelman M. C., McKee C. F., 1990, *ApJ*, **358**, 375
- Binney J., Merrifield M., 1998, *Galactic Astronomy*
- Bisnovatyi-Kogan G. S., Lovelace R. V. E., 1997, *ApJ*, **486**, L43
- Burkert A., Lin D. N. C., 2000, *ApJ*, **537**, 270
- Celotti A., Rees M. J., 1999, *MNRAS*, **305**, L41
- Chatzopoulos S., Fritz T. K., Gerhard O., Gillessen S., Wegg C., Genzel R., Pfuhl O., 2015, *MNRAS*, **447**, 948
- Cid Fernandes R., Mateus A., Sodré L., Stasinska G., Gomes J. M., 2011, *STARLIGHT: Spectral Synthesis Code, Astrophysics Source Code Library* (ascl:1108.006)
- Ciotti L., Ostriker J. P., 2001, *ApJ*, **551**, 131
- Ciotti L., Ostriker J. P., 2007, *ApJ*, **665**, 1038
- Cole D. R., Debattista V. P., 2016, *Galactic Bulges*, **418**, 107
- Cox D. P., 2005, *ARA&A*, **43**, 337
- Czerny B., Karas V., Kunneriath D., Das T. K., 2013a, in Zhang C. M., Belloni T., Méndez M., Zhang S. N., eds, *IAU Symposium Vol. 290, IAU Symposium*. pp 199–200 ([arXiv:1211.1226](https://arxiv.org/abs/1211.1226)), [doi:10.1017/S1743921312019606](https://doi.org/10.1017/S1743921312019606)
- Czerny B., Kunneriath D., Karas V., Das T. K., 2013b, *A&A*, **555**, A97
- Dale J. E., 2015, *New Astron. Rev.*, **68**, 1
- Defouw R. J., 1970, *ApJ*, **160**, 659
- Dopita M. A., Sutherland R. S., 2003, *Astrophysics of the diffuse universe*
- Draine B. T., Giuliani Jr. J. L., 1984, *ApJ*, **281**, 690
- Dyson J. E., Williams D. A., 1980, *Physics of the interstellar medium*
- Eckart A., Schödel R., Straubmeier C., 2005, *The black hole at the center of the Milky Way*
- Fabian A. C., 2012, *ARA&A*, **50**, 455
- Fellhauer M., Kroupa P., 2006, *MNRAS*, **367**, 1577
- Ferland G., 1996, *Department of Physics and Astronomy Internal Report*, **1**, 1
- Ferland G. J., et al., 2013, *Rev. Mex. Astron. Astrofis.*, **49**, 137
- Field G. B., 1965, *ApJ*, **142**, 531
- Frank J., Gisler G., 1976, *MNRAS*, **176**, 533
- Fritz T. K., et al., 2016, *ApJ*, **821**, 44
- Genzel R., Eisenhauer F., Gillessen S., 2010, *Reviews of Modern Physics*, **82**, 3121
- Gezari D. Y., Shu P., Lamb G., Tresch-Fienberg R., Fazio G. G., Hoffmann W. F., Gatley I., McCreight C., 1985, *ApJ*, **299**, 1007
- Hueytol-Zahuantitla F., Palouš J., Wunsch R., Tenorio-Tagle G., Silich S., 2013, *ApJ*, **766**, 92
- Kennicutt R. C., 1998, *ARA&A*, **36**, 189
- Kennicutt R. C., Evans N. J., 2012, *ARA&A*, **50**, 531
- Kennicutt R. C., Schweizer F., Barnes J. E., Friedli D., Martinet L., Pfenniger D., eds, 1998, *Galaxies: Interactions and Induced Star Formation*
- Khajenabi F., Rahmani M., 2015, *Research in Astronomy and Astrophysics*, **15**, 2187
- Klessen R. S., Glover S. C. O., 2016, *Star Formation in Galaxy Evolution: Connecting Numerical Models to Reality, Saas-Fee Advanced Course, Volume 43*. ISBN 978-3-662-47889-9. Springer-Verlag Berlin Heidelberg, 2016, p.~85, 43, 85
- Krolik J. H., McKee C. F., Tarter C. B., 1981, *ApJ*, **249**, 422
- Langer W. D., 1978, *ApJ*, **225**, 95
- Leitherer C., et al., 1999, *ApJS*, **123**, 3
- Lu J. R., Do T., Ghez A. M., Morris M. R., Yelda S., Matthews K., 2013, *ApJ*, **764**, 155
- Luo B., et al., 2013, *ApJS*, **204**, 14
- McCourt M., Sharma P., Quataert E., Parrish I. J., 2012, *MNRAS*, **419**, 3319
- Mieske S., 2014, in *Revista Mexicana de Astronomía y Astrofísica Conference Series*. pp 181–182
- Mieske S., Frank M. J., Baumgardt H., Lützgendorf N., Neumayer N., Hilker M., 2013, *A&A*, **558**, A14
- Moore K., Bildsten L., 2011, *ApJ*, **728**, 81
- Moscibrodzka M., 2006, *A&A*, **450**, 93

- Mościbrodzka M., Proga D., 2013, *ApJ*, **767**, 156
- Mościbrodzka M., Gammie C. F., Dolence J. C., Shiokawa H., Leung P. K., 2009, *ApJ*, **706**, 497
- Mościbrodzka M., Shiokawa H., Gammie C. F., Dolence J. C., 2012, *ApJ*, **752**, L1
- Parrish I. J., Quataert E., Sharma P., 2009, *ApJ*, **703**, 96
- Pellegrini S., 2012, in Kim D.-W., Pellegrini S., eds, *Astrophysics and Space Science Library* Vol. 378, *Astrophysics and Space Science Library*, p. 21 ([arXiv:1112.2140](#)), doi:10.1007/978-1-4614-0580-1_2
- Pellegrini S., Ciotti L., Ostriker J. P., 2012, *ApJ*, **744**, 21
- Plewa T., 1995, *MNRAS*, **275**, 143
- Ponti G., Terrier R., Goldwurm A., Belanger G., Trap G., 2010, *ApJ*, **714**, 732
- Quataert E., 2004, *ApJ*, **613**, 322
- Reines A. E., 2014, *Nature*, **513**, 322
- Róžańska A., Czerny B., 1996, *Acta Astron.*, **46**, 233
- Róžańska A., Czerny B., Kunneriath D., Adhikari T. P., Karas V., Mościbrodzka M., 2014, *MNRAS*, **445**, 4385
- Róžańska A., Mróz P., Mościbrodzka M., Sobolewska M., Adhikari T. P., 2015, *A&A*, **581**, A64
- Scannapieco E., Brüggen M., 2015, *ApJ*, **805**, 158
- Schartmann M., Meisenheimer K., Klahr H., Camenzind M., Wolf S., Henning T., 2009, *MNRAS*, **393**, 759
- Schödel R., Feldmeier A., Kunneriath D., Stolovy S., Neumayer N., Amaro-Seoane P., Nishiyama S., 2014, *A&A*, **566**, A47
- Seth A. C., et al., 2014, *Nature*, **513**, 398
- Sharma P., McCourt M., Quataert E., Parrish I. J., 2012, *MNRAS*, **420**, 3174
- Shcherbakov R. V., Baganoff F. K., 2010, *ApJ*, **716**, 504
- Shcherbakov R. V., Wong K.-W., Irwin J. A., Reynolds C. S., 2014, *ApJ*, **782**, 103
- Silich S., Tenorio-Tagle G., Rodríguez-González A., 2004, *ApJ*, **610**, 226
- Silich S., Tenorio-Tagle G., Hueyotl-Zahuantitla F., 2008, *ApJ*, **686**, 172
- Strader J., et al., 2013, *ApJ*, **775**, L6
- Swamy K. S. K., 2005, *Dust In The Universe: World Scientific Series in Astronomy and Astrophysics*, vol.~7, 7
- Tacchella S., et al., 2015, *Science*, **348**, 314
- Tarter C. B., Tucker W. H., Salpeter E. E., 1969, *ApJ*, **156**, 943
- Tenorio-Tagle G., Silich S., Martínez-González S., Muñoz-Tuñón C., Palouš J., Wünsch R., 2013, *ApJ*, **778**, 159
- Wang J.-M., Cheng C., Li Y.-R., 2012, *ApJ*, **748**, 147
- Wang Q. D., et al., 2013, *Science*, **341**, 981
- Yuan F., Narayan R., 2014, *ARA&A*, **52**, 529
- Zhang H.-X., et al., 2015a, *ApJ*, **802**, 30
- Zhang S., et al., 2015b, *ApJ*, **815**, 132
- de Grijs R., Lépine J. R. D., eds, 2010, *Star Clusters: Basic Galactic Building Blocks Throughout Time and Space IAU Symposium* Vol. 266
- van Hoven G., Mok Y., 1984, *ApJ*, **282**, 267